LBL-7167

Heavy Ion Reactions in the Transition Region

David L. Hendrie

(Invited Paper at the International Symposium
on Nuclear Physics at Cyclotron Energies
Calcutta, India, Sept. 14-16, 1977)

Abstract

Evidence is given for a serious and systematic failure of the DWBA to predict the cross sections for single nucleon transfers induced by heavy ions above about 10 MeV/Nucleon beam energies. This is perhaps related to a coherent coupling to a increasing cross section to the quasi-elastic continuum, which also shows an anomalous energy dependence at about the same energy.

NOTICE

This report was prepared as an account of work sponsored by the United States Government. Neither the United States nor the United States Department of Energy, nor any of their employees, nor any of their contractors, subcontractors, or their employees, makes any warranty, express or implied, or assumes any legal liability or responsibility for the accuracy, completeness or usefulness of any information, apparatus, product or process disclosed, or represents that its use would not infringe privately owned rights.

Work performed under the auspices of the U. S. Department of Energy.

This presentation has been prepared to show the work that has been going on at the Berkeley 88-Inch Cyclotron in the field of heavy ion reactions. The work has proceeded from rather traditional one-nuclear transfer reactions to known sharp final states, to massive transfers into the continuum. Both of these reactions are revealing that something new is going on at energies above about 10 MeV/A, which was not expected from work at lower energies, and which is not yet fully understood.

Figure 1 shows a spectrum of excited states in ^{209}Bi made by a beam of 312 MeV ^{16}O, and measured by detecting the outgoing ^{15}N in the Berkeley QSD spectrometer.[1] The well known single particle states of ^{209}Bi have been well studied by a variety of light ion transfer reactions, as well as at lower bombarding energies[2] at Berkeley as seen in fig. 2. From these other reactions, and from shell model structure calculations, the wave functions of these states and the spectroscopic factors (which are close to unity) have seemingly been well determined. Even as a function of energy, the relative excitation of the states agrees well with calculations of a sophisticated DWBA transfer code such as PTOLEMY, which includes higher order effects such a finite range recoil term.[3] The shifting of strength from the $f_{7/2}$ non-spin-flip to the $f_{5/2}$ spin-flip state, for example, is predicted by the model. The employment of the DWBA model follows the usual prescription of determining the scattering distorted waves from optical model parameters obtained for fits to appropriate elastic scattering data (fig. 3). Straight forward application of the model then provides a good description of the angular distributions (fig. 4) and relative excitations of the states in ^{209}Bi.

However, as a function of energy, the model begins to seriously fail in the prediction of the absolute cross sections (fig. 5). Up to an energy of 140 MeV (including data from ref. 4 at an energy below the Coulomb barrier, where optical potentials are not a factor), the model and data agree. At higher energies, however, the model overpredicts the measured cross section by up to a factor of 5 or 6. No reasonable alteration of optical model parameters, using energy independent or smoothly energy dependent prescriptions, can essentially alter the predictions. Nor does it change by attempts to alter the description of the bound state wave function, provided we maintain agreement with the low energy and light ion transfer data, and with structure calculations. Use of a two-center shell model approach[5] does not help, because it affects mainly the low energy predictions. A comparable breakdown of the DWBA predictions is also observed in neutron transfer reactions, eliminating coulomb effects as a probable cause.

What is the reason for this unexpected and catastrophic failure of the model. At this point, we do not know but are considering the following possibilities, none of which seem completely satisfactory.

1) The bound state wave function contains two many high momentum components, facilitating the transfer at high energies. Some simple ways of estimating this possibility gave rise to a 20% change, instead of the factor of 5-6 needed.

2) There is a possibility of an energy dependence implicit in the DWBA which is not explicitly carried in the formalism.[6] This effect is estimated by theoretical means to be rather small.

3) Coupled-channel effects to collectively enhanced bound states, especially in the projectile system, might have a much stronger energy dependence than expected. This seems unlikely but the relevant calculations have not yet been completed.

4) Lastly, a coherent coupling to a new channel which increases strongly with energy. Such a possible channel can be seen as a strength, growing with energy, in the continuum region above an excitation energy of about 8 MeV. Although the origin of the needed coherence is not apparent, the investigation of the transfer into the continuum "Quasi-elastic" peak has proven to be a fascinating subject in its own right.

Focussing our attention on transfer reactions to the continua gave rise to energy spectra such as shown in fig. 6. Because we were interested in a wide range of particle types and energies from the reaction, and were less interested in energy resolution, we performed the massive transfer work using solid state detector telescopes. This had the disadvantageous side effect of worsening the particle identification resolution, so that we could not always reliably separate the isotopic composition of elemental yields. Figure 6, for example, shows the yield for each element summed over all isotopes. However, enough cases with isotopic separation were available to confirm that the following discussion is consistent with isotopic, as well as elemental yields. We will focus our attention on the large peak in the spectra, which we will call, traditionally if somewhat arbitrarily, the quasi-elastic peak. This is to be distinguished

from (experimentally if not conceptually) the deep-inelastic results which are better observed with heavier projectiles and at lower bombarding energy per nucleon, and which gives rise to a peak near the Coulomb barrier, marked V_c on the figure.

To provide a context for understanding our results, I wish to digress a moment and summarize some results[7] of the Heckman group at the LBL Bevalac. Their experiment was similar, using a 1.05 and 2.1 GeV/A beam of ^{16}O on several targets, and looking at isotopic yields and energy (or momentum) spreads of outgoing particles with energy per nucleon about the same as the beam. (At these energies, the angular distribution essentially collapses to zero degrees). They reported that their momentum spreads are predicted by a fast knock out of the observed cluster[8] having the expected Fermi motion when bound in the projectile. In addition, their isotopic yields were explained by this picture. The observed independence of results on target species and beam energy are also consistent.

An alternative explanation involved a two stage mechanism,[9] with excitation of the projectile during the collision and its subsequent decay, with sufficient time elapsed for the projectile to thermalize at some temperature T, calculated to be 7 to 8 MeV. This model also explained both yields and widths. It was also shown[10] that the two models give the same results, with the yields proportional to

$$Y \sim e^{-Q/T} \qquad (1)$$

where Q is the binding energy of the fragment and T is the temperature, or is a constant which can be simply related to the Fermi momentum of the cluster using a well known prescription.

In fig. 7, we compare the yields at 315 MeV with those at 33.6 GeV and see that, although there is a systematic isotopic difference, the elemental yields[11] have a constant ratio of 1.7 to 1. Figure 8 shows that target independence also holds at 315 MeV. Fitting the widths of the Quasi-elastic peaks with the Fermi motion, or temperature, averaged over isotopes, gives the solid lines on fig. 5. The expected location of the peaks is marked by the arrows E_F, determined from the binding energies (and small kinematic effect) for a pure fragmentation process. Further, under the assumption that the decay or fragmentation process is isotropic, (fig. 9) we can also fit the angular distributions at 315 MeV.[12] The evidence seems overwhelming that we are observing comparable processes at 315 MeV and 33.6 GeV. This is somewhat modified by evidence from coincidence work[13] of significant contributions from $^{13}C + \alpha$, $^{14}C + \alpha$, and $^{14}N + \alpha$, that the 315 MeV result cannot be quite so simply related, since the pick-up plus fragmentation mechanism is expected not to contribute at 33.6 GeV.[14] Nevertheless, the major conclusion remains.

It is tempting to try the analysis at a lower energy. At 140 MeV the spectra are qualitatively similar to those at 315; the peak location is still well determined by fragmentation Q-values. However, the width of the peaks no longer correspond to Fermi velocities. Figure 11 shows that the yields are no longer in constant ratio to those at higher energies, and fig. 12 shows that target independence also no longer applies. We can no longer obtain a consistent temperature using the previous ideas. Something seems to have drastically changed.

We can improve things, however, still using eq. 1. Following an idea of Volkov[15] based on a deep-inelastic concept, we use two-body ground state Q-values in eq. 1, instead of the fragmentation Q-values used before. Plotting yields vs. Q_{gg} gives us (fig. 13) a temperature of about 2 MeV. Using Q_{gg} at higher energies does equally poorly as using Q fragmentation at 140 MeV.

In order to fill out the picture we have taken data at intermediate energies at the cyclotron (fig. 14) and at 80 MeV/A at the Bevalac. Preliminary results from on-going coincidence studies tends to confirm our deductions, that the fragments came from the projectile and that little excitation energy is involved. Of course, we expect ultimately to learn much more.

A summary of the results is shown in fig 15, where we have chosen to plot, as a function of incident energy, a characteristic temperature derived both from yields and peak widths, including data not our own.[7,15] This shows immediately the anomalous behavior of the production mechanism at 315 MeV. A tentative explanation for the sharp rise in temperature at 315 is that a speed of the reaction has been obtained that is too fast for the complex to equilibrate. We simply estimate that time to be about $1\text{-}2 \times 10^{-22}$ seconds. The saturation of the temperature at 8 MeV can possibly be considered as a phase transition ie., the point at which particle emission would cool the projectile.

It is clear that we have identified two problems much better than we have determined their solutions. Some of conclusions are not only conjectural, but non-quantitative. We are not sure the two anomalies are connected. We are surprised to find these effects at

such low energies, since a characteristic nucleon velocity at the nuclear surface is expected to be at an equivalent energy of 30 to 50 MeV per nucleon. We are hoping that coincidence measurements underway can help specify the reaction more precisely. A deeper understanding of the relationship of temperature and nucleon Fermi motion is required, as is an extension of traditional dynamic model, such as the DWBA, to unbound continuum states, so as to unify the description of the different reactions.

I wish to acknowledge the invaluable roles played by many experimental and theoretical collaborators. Especially the paramount contributions of D. S. Scott to the experiments and to the concepts cannot be over emphasized.

References

1. C. Olmer, M. C. Mermaz, M. Buenerd, C. K. Gelbke, D. L. Hendrie, J. Mahoney, A. Menchaca-Rocha, D. K. Scott, M. H. MacFarlane, and S. C. Pieper. Phys. Rev. Letters 38, 476 (1977).
2. S. C. Pieper, M. H. MacFarlane, D. H. Gloeckner, D. G. Kovar, F. D. Becchetti, B. G. Harvey, D. L. Hendrie, H. Homeyer, J. Mahoney, F. Puhlhofer, W. von Oertzen, and M. Zisman. Submitted to Phys. Rev. C.
3. C. Olmer, M. Mermaz, M. Buenerd, C. K. Gelbke, D. L. Hendrie, J. Mahoney, D. K. Scott, M. H. MacFarlane and S. C. Pieper. LBL-6553 (July 1977), (to be published).
4. A. R. Barnett, W. R. Phillips, P. J. A. Buttle, and L. J. B. Goldfarb. Nucl. Phys. 176, 321 (1971).
5. K. Pruess, G. Delic, L. A. Charlton, and N. K. Glendenning. Proceedings of the Symposium on Macroscopic Features of Heavy-Ion Collisions, Argonne National Laboratory Report ANL/PHY-76-2, p. 723.
6. R. M. Thaler (Private Communication).
7. D. L. Greiner, P. J. Lindstrom, H. H. Heckman, B. Cork and F. S. Bieser, Phys. Rev. Lett. 35 (1975) 152.
8. H. Feshbach and K. Huang, Phys. Lett. 47B (1973) 300.
9. V. K. Lukyanov and A. I. Titov, Phys. Lett. 57B (1975) 10.
10. A. S. Goldhaber, Phys. Lett. 53B (1974) 306.
11. M. Buenerd, C. K. Gelbke, B. G. Harvey, D. L. Hendrie, J. Mahoney, A. Menchaca-Rocha, C. Olmer, and D. K. Scott, Phys. Rev. Lett. 37, 1191 (1976); C. K. Gelbke, M. Buenerd, D. L. Hendrie, J. Mahoney, M. C. Mermaz, C. Olmer, and D. K. Scott. Phys. Lett. 65B, 227 (1976).
12. C. K. Gelbke, D. K. Scott, M. Bini, D. L. Hendrie, J. L. LaVille, J. Mahoney, M. C. Mermaz, and C. Olmer. (To be published in Phys. Letters).
13. C. K. Gelbke, M. Bini, C. Olmer, D. L. Hendrie, J. L. LaVille, J. Mahoney, M. C. Mermaz, D. K. Scott and H. H. Wieman. (To be published in Phys. Letters).
14. J. Hufner, C. Sander, and G. Wolshin. (To Be Published).
15. V. V. Volkov in Classical and Quantum Mechanical Aspects of Heavy-Ion Collisions, H. L. Harney, P. Braun-Munzinger, and C. K. Gelbke, eds., (Springer-Verlag, Heidelberg, 1975), p. 253.

Figure Captions

Fig. 1. Energy spectrum obtained at the laboratory angle of 11.9° for the reaction $^{208}Pb(^{16}O,^{15}N)^{209}Bi$. Transitions to known single-particle states in ^{209}Bi are identified.

Fig. 2. Energy spectra obtained for the $^{208}Pb(^{16}O,^{15}N)^{209}Bi$ reaction at incident energies of 104, 138.5, 216.6 and 312.6 MeV. Transitions to known proton single-particle states are labeled according to their shell-model orbitals.

Fig. 3. Elastic scattering angular distributions for 312.6 MeV ^{16}O on ^{208}Pb. The curve is an optical model fit.

Fig. 4. Differential cross sections for the reaction $^{208}Pb(^{16}O,^{15}N)$ ^{209}Bi populating the $h_{9/2}$ ground state at an incident energy of 104, 140, 216.6 and 312.6 MeV, from right to left. The solid lines are DWBA calculations described in the text.

Fig. 5. Experimental and DWBA angle-integrated cross sections for the $^{208}Pb(^{16}O,^{15}N)^{209}Bi$ reaction as a function of incident energy. The curves for two optical potentials, both using spectroscopic factors from structure calculations are shown.

Fig. 6. Energy spectra of reaction products N, C, B, Be, Li measured in the bombardment of ^{208}Pb by ^{16}O-ions of 315 MeV at the laboratory angle of 15°. The dotted curves are calculated as explained in the text. The arrows denoted by V_C and E_F correspond to the exit-channel Coulomb barrier and the energy predicted for a fragmentation of the projectile into the observed fragment together with individual nucleons and alpha particles.

Fig. 7. Ratios of cross sections measured for the reactions ^{16}O + ^{208}Pb at 315 MeV and 33.6 GeV laboratory energies.

Fig. 8. Comparison of Isotopic yields seen in the bombardment of several targets by 315 MeV ^{16}O ions.

Fig. 9. Angular distributions [10] of reaction products N, C, B, Be, Li measured in the bombardment of ^{208}Pb by ^{16}O ions of 315 MeV. The curves are calculated assuming isotropic decay as explained in the text.

Fig. 10. Energy spectra of the elements nitrogen, carbon, boron, beryllium, and lithium produced in the reaction ^{16}O + ^{208}Pb at $\Theta_L = 40°$ and $E_L = 140$ MeV. The arrows marked by g.s., E_P, V_C and E_F correspond to the energy of the ground-state transition for a two-body transfer reaction, the energy of a reaction product with the projectile velocity, the exit-channel Coulomb barrier, and the energy predicted for a fragmentation of the projectile by the channel with minimum A-value, respectively.

Fig. 11. Ratios of isotope and element production cross sections induced by 140 MeV and 315 MeV ^{16}O ions on ^{203}Pb.

Fig. 12. Comparison of isotope yields observed in the bombardment of ^{208}Pb, ^{197}Au, and ^{94}Zr targets by ^{16}O at 140 MeV laboratory energy.

Fig. 13. Isotope-production cross sections observed for reactions inducted by ^{16}O on ^{208}Pb at the laboratory angle $\Theta_L = 40°$ and 140 MeV incident energy. The dependence on the ground-state Q-value, Q_{gg}, of the corresponding transfer reaction is shown.

Fig. 14. A plot of energy spectra of the (^{16}O,^{12}C) reaction at 4 incident energies. E_F and E_F' correspond to minimum and maximum fragmentation energies, respectively and E_p is the energy corresponding to beam velocity. The curves are fitted gausian used to derive temperature described inthe text.

Fig. 15. A plot of temperatures derived from yields and peak widths as described in the text. The solid line is a predicted temperature from low energy work, the dashed line is only to guide the eye. Data from refs. 7 and 15 are included. Some of the results are to be considered preliminary.

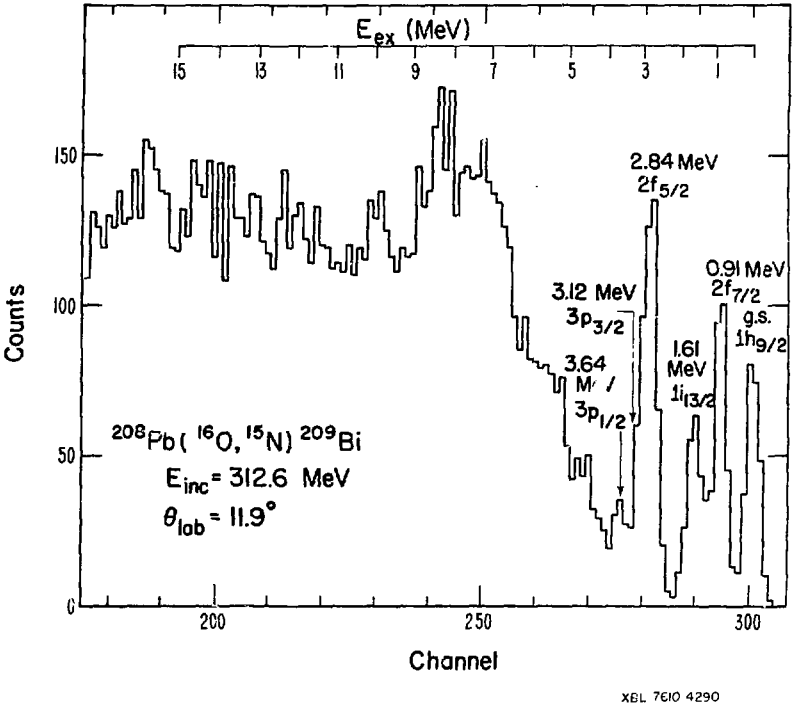
E_ex (MeV)
15
13
11
9
7
5
3
1
150
100
50
0
Counts
2.84 MeV
2f5/2
0.91 MeV
2f7/2
g.s.
1h9/2
3.12 MeV
3p3/2
3.64
3p1/2
1.61
MeV
1i13/2
208Pb(16O, 15N) 209Bi
Einc = 312.6 MeV
θlab = 11.9°
200
250
300
Channel
XBL 7610 4290

Fig. 1

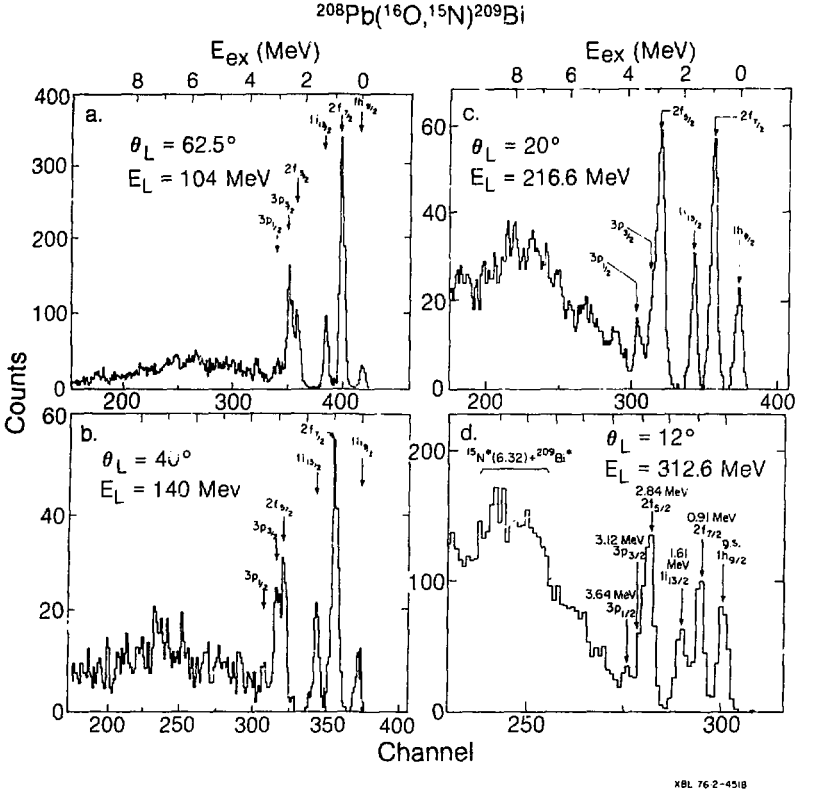
208Pb(16O,15N)209Bi
Eex (MeV)
Counts
Channel
a.
θL = 62.5°
EL = 104 MeV
b.
θL = 40°
EL = 140 Mev
c.
θL = 20°
EL = 216.6 MeV
d.
θL = 12°
EL = 312.6 MeV
15N*(6.32)+209Bi*
2.84 MeV
0.91 MeV
g.s.
3.12 MeV
1.61 MeV
3.64 MeV
XBL 762-4518

Fig. 2

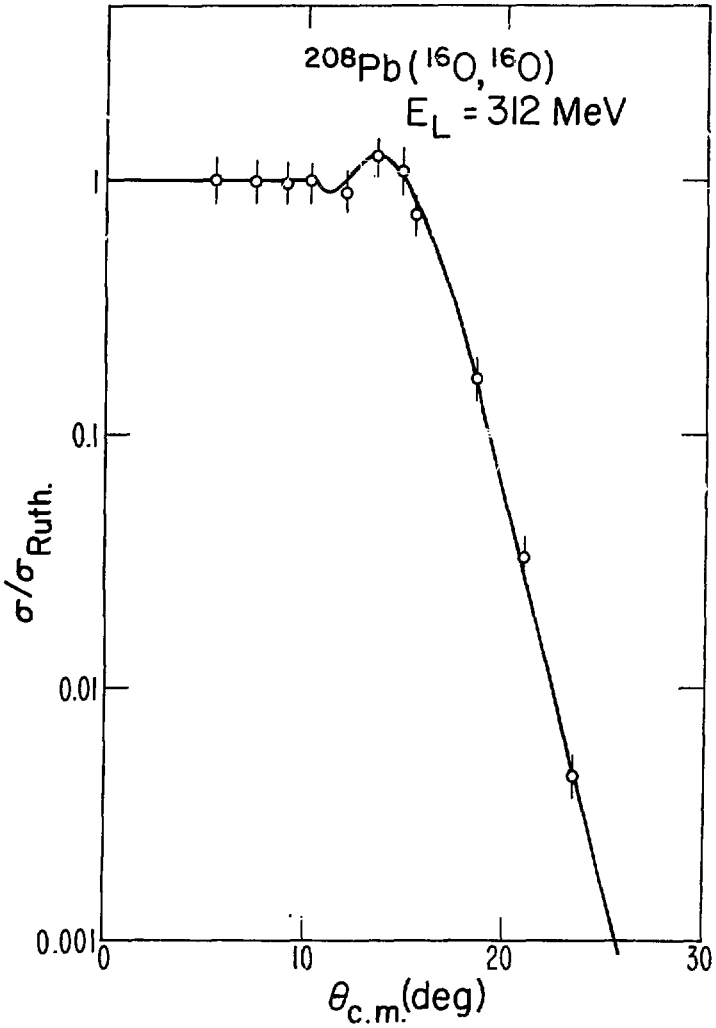

XBL 7610 4137

Fig. 3

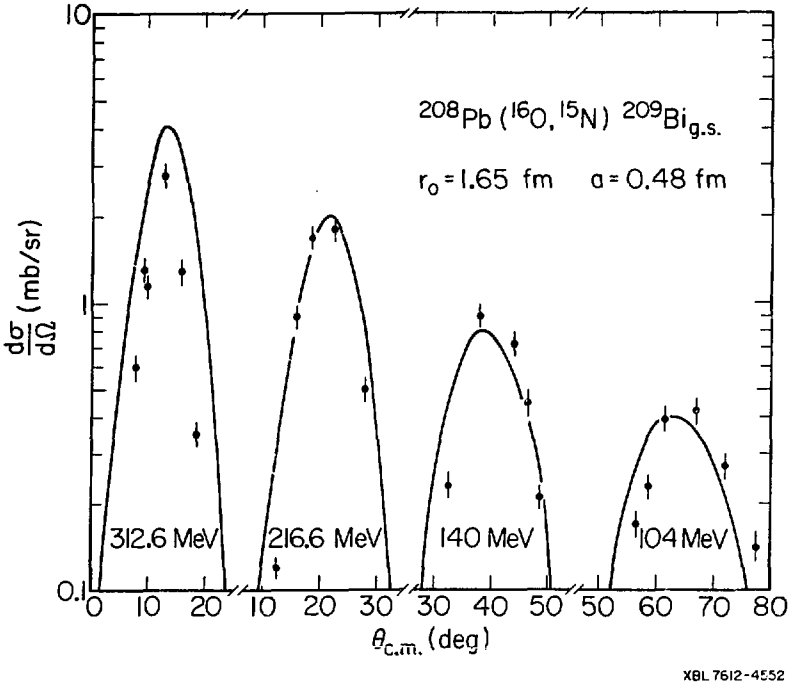
$^{208}Pb(^{16}O,^{15}N)\ ^{209}Bi_{g.s.}$
$r_0 = 1.65$ fm $a = 0.48$ fm
312.6 MeV
216.6 MeV
140 MeV
104 MeV
$\frac{d\sigma}{d\Omega}$ (mb/sr)
$\theta_{c.m.}$ (deg)
10
1
0.1
0 10 20 10 20 30 30 40 50 50 60 70 80
XBL 7612-4552

Fig. 4

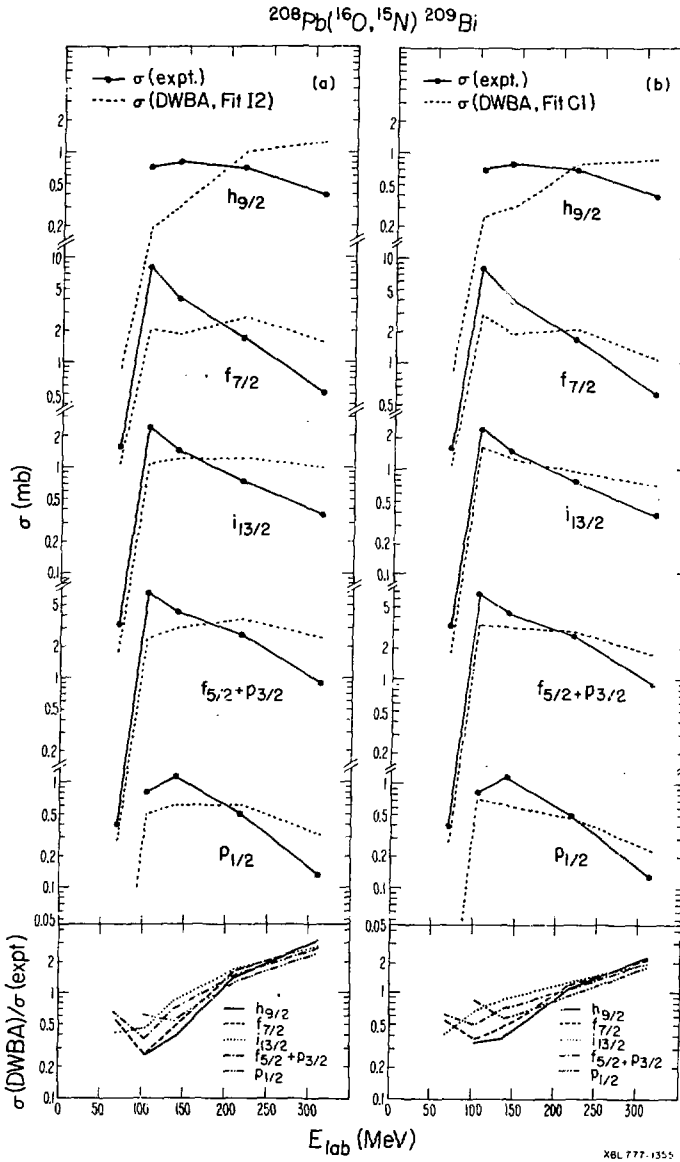
$^{208}Pb(^{16}O,^{15}N)\,^{209}Bi$
σ (expt.)
σ (DWBA, Fit I2)
(a)
σ (expt.)
σ (DWBA, Fit C1)
(b)
$h_{9/2}$
$f_{7/2}$
$i_{13/2}$
$f_{5/2}+p_{3/2}$
$p_{1/2}$
σ (mb)
σ(DWBA)/σ (expt)
E_{lab} (MeV)
XBL 777-1355

Fig. 5

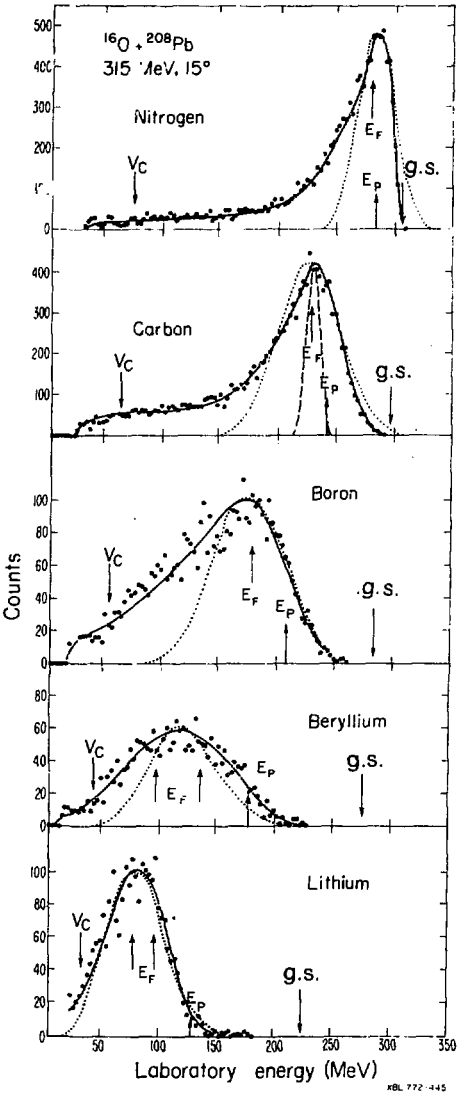
$^{16}O + ^{208}Pb$
315 MeV, 15°
Nitrogen
Carbon
Boron
Beryllium
Lithium
V_C
E_F
E_P
g.s.
Counts
Laboratory energy (MeV)
XBL 772-445

Fig. 6

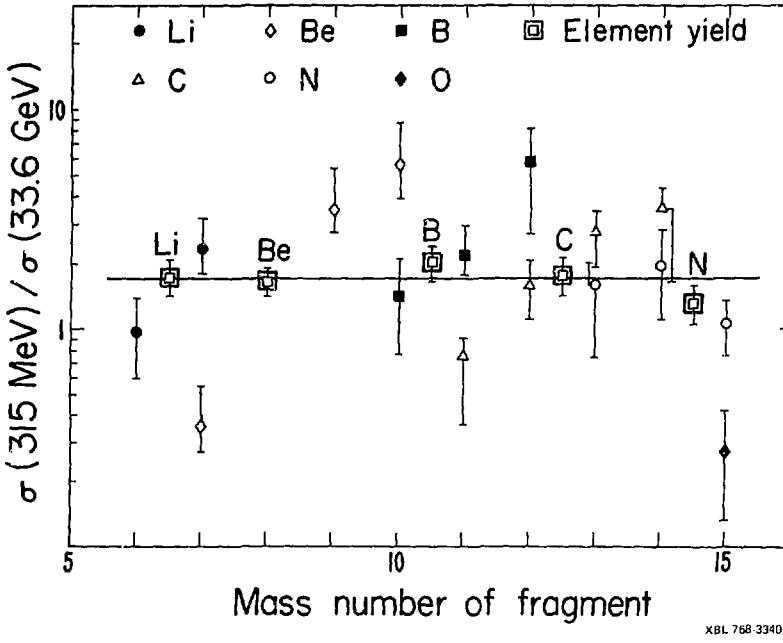
Li
Be
B
Element yield
C
N
O
Li
Be
B
C
N
10
1
5
10
15
σ (315 MeV) / σ (33.6 GeV)
Mass number of fragment
XBL 768-3340

Fig. 7

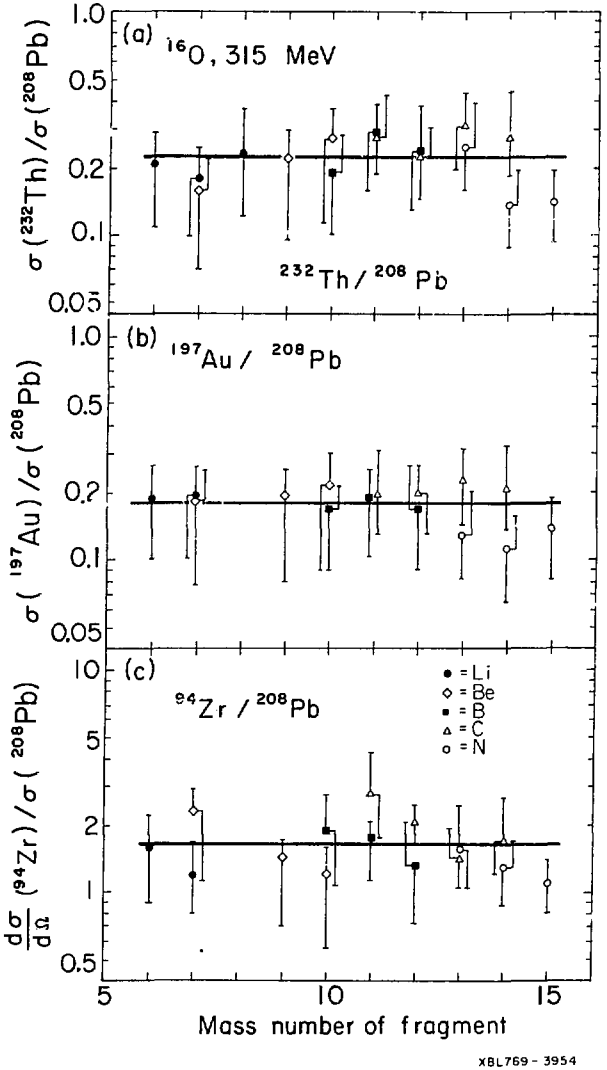
(a) ^{16}O, 315 MeV
$\sigma(^{232}Th)/\sigma(^{208}Pb)$
^{232}Th / ^{208}Pb
(b) ^{197}Au / ^{208}Pb
$\sigma(^{197}Au)/\sigma(^{208}Pb)$
(c) ^{94}Zr / ^{208}Pb
$\frac{d\sigma}{d\Omega}(^{94}Zr)/\sigma(^{208}Pb)$
● = Li
◇ = Be
■ = B
△ = C
○ = N
Mass number of fragment
XBL769-3954

Fig. 8

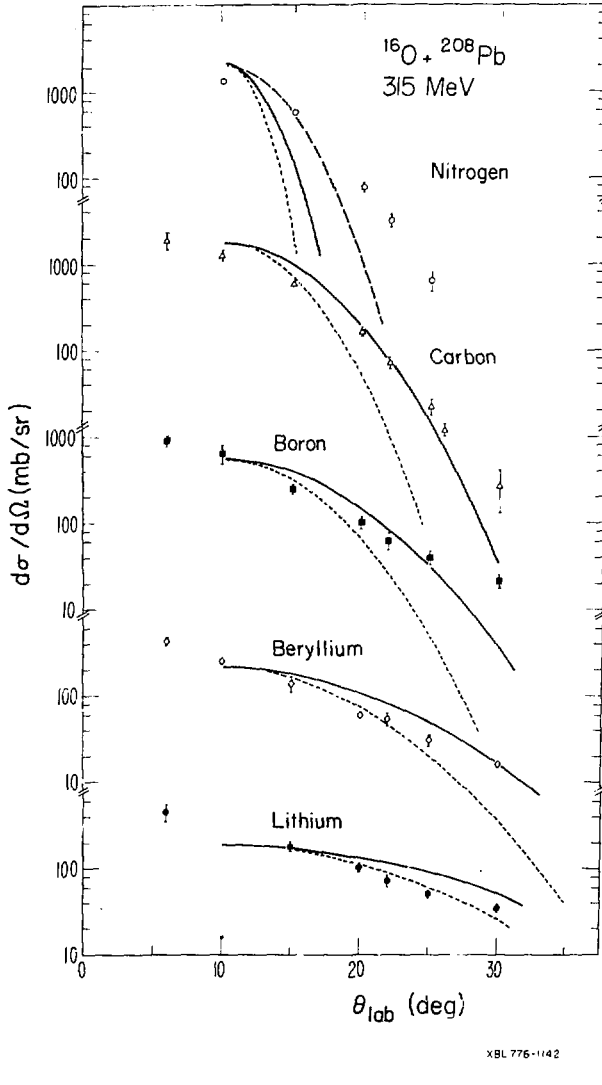
$^{16}O + ^{208}Pb$
315 MeV
Nitrogen
Carbon
Boron
Beryllium
Lithium
1000
100
10
0
10
20
30
$d\sigma/d\Omega$ (mb/sr)
θ_{lab} (deg)
XBL 776-1142

Fig. 9

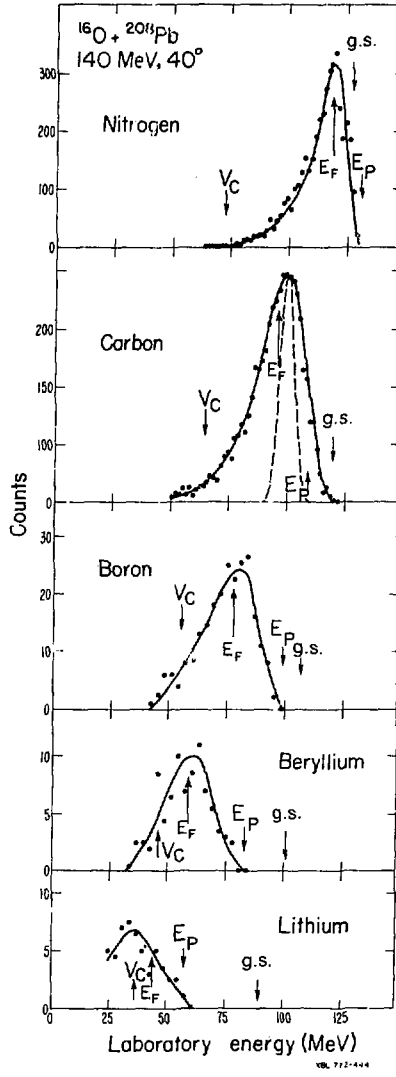
$^{16}O + ^{208}Pb$
140 MeV, 40°
Nitrogen
Carbon
Boron
Beryllium
Lithium
g.s.
V_C
E_F
E_P
Counts
Laboratory energy (MeV)
0
25
50
75
100
125

Fig. 10

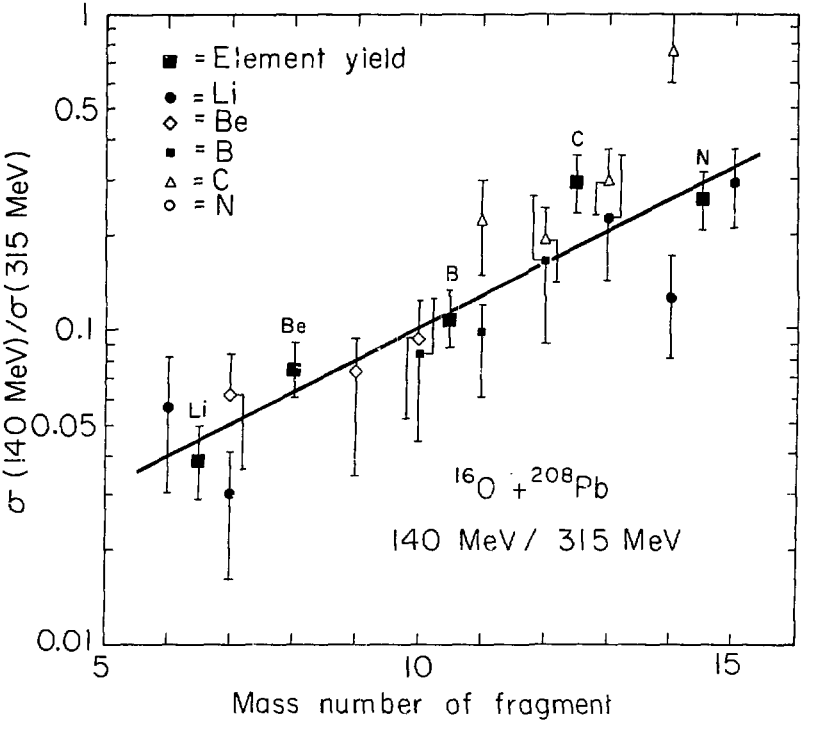

XBL769-3952

Fig. 11

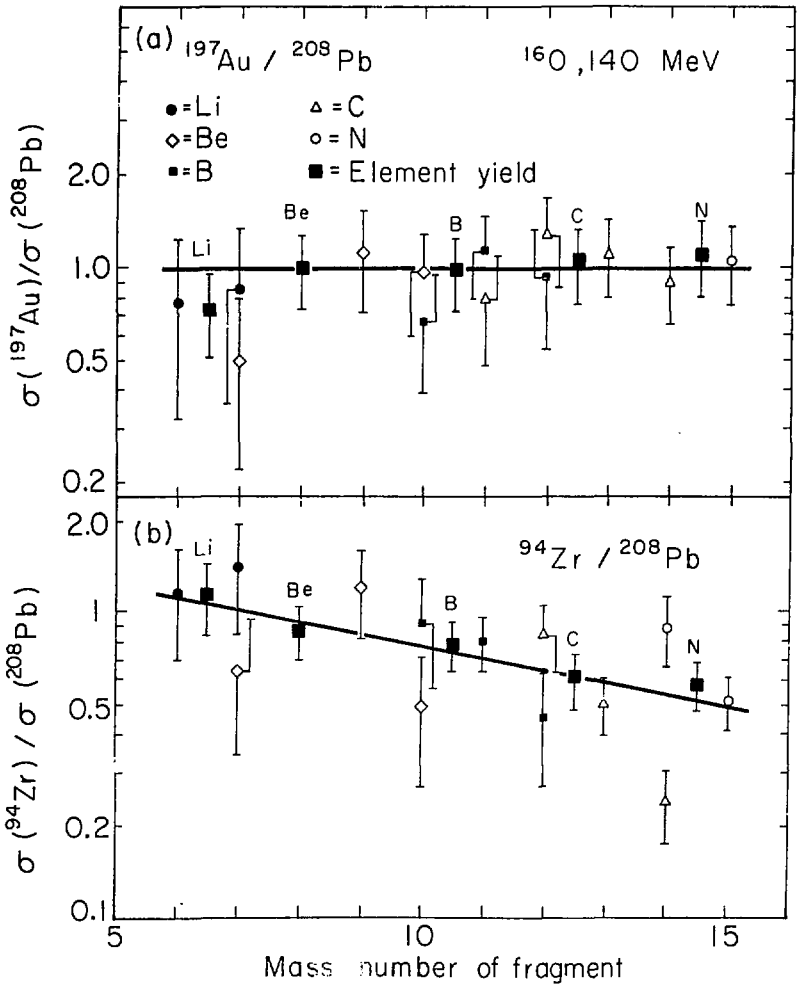

XBL769-3949

Fig. 12

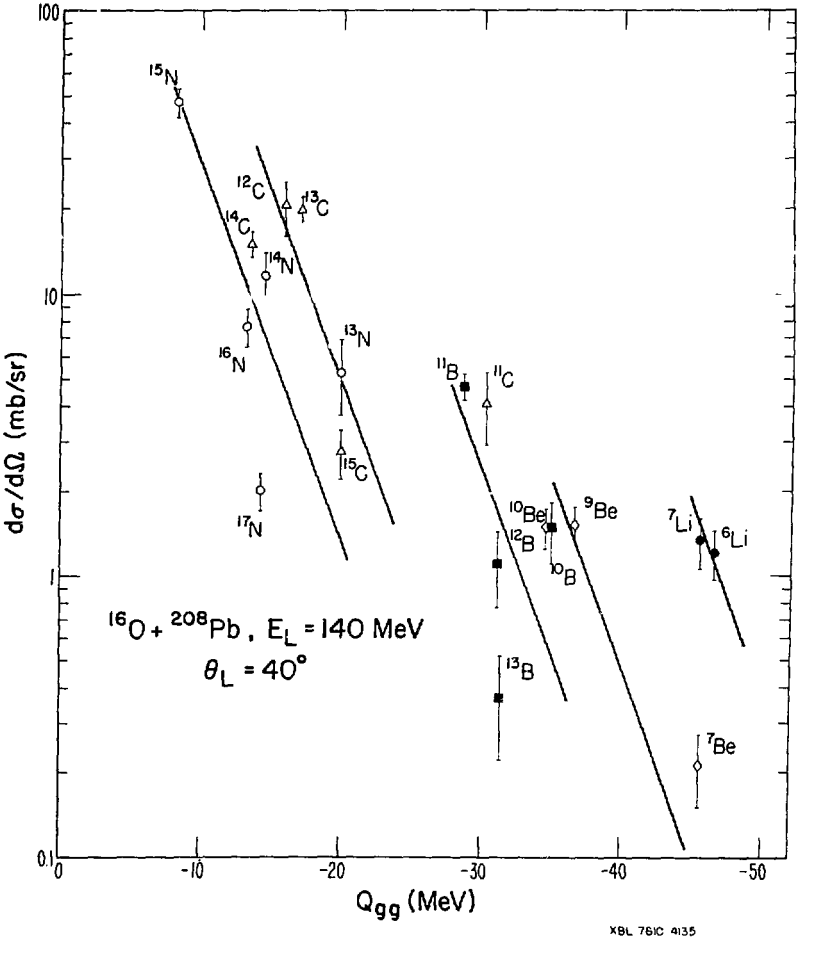
100
10
1
0.1
dσ/dΩ (mb/sr)
0
-10
-20
-30
-40
-50
Qgg (MeV)
15N
12C
13C
14C
14N
16N
13N
15C
17N
11B
11C
10Be
9Be
12B
10B
13B
7Li
6Li
7Be
16O + 208Pb , EL = 140 MeV
θL = 40°
XBL 761C 4135

Fig. 13

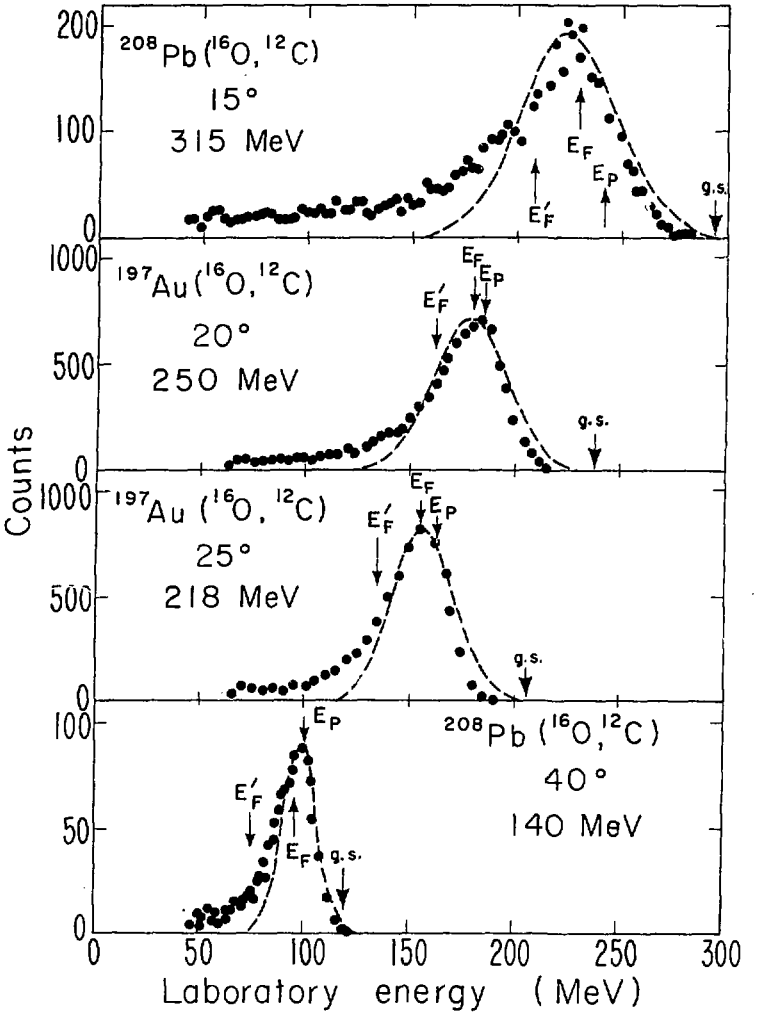
^{208}Pb(^{16}O,^{12}C)
15°
315 MeV
E_F
E_P
E'_F
g.s.
^{197}Au(^{16}O,^{12}C)
20°
250 MeV
^{197}Au (^{16}O, ^{12}C)
25°
218 MeV
^{208}Pb (^{16}O,^{12}C)
40°
140 MeV
Counts
Laboratory energy (MeV)
XBL7711-11041

Fig. 14

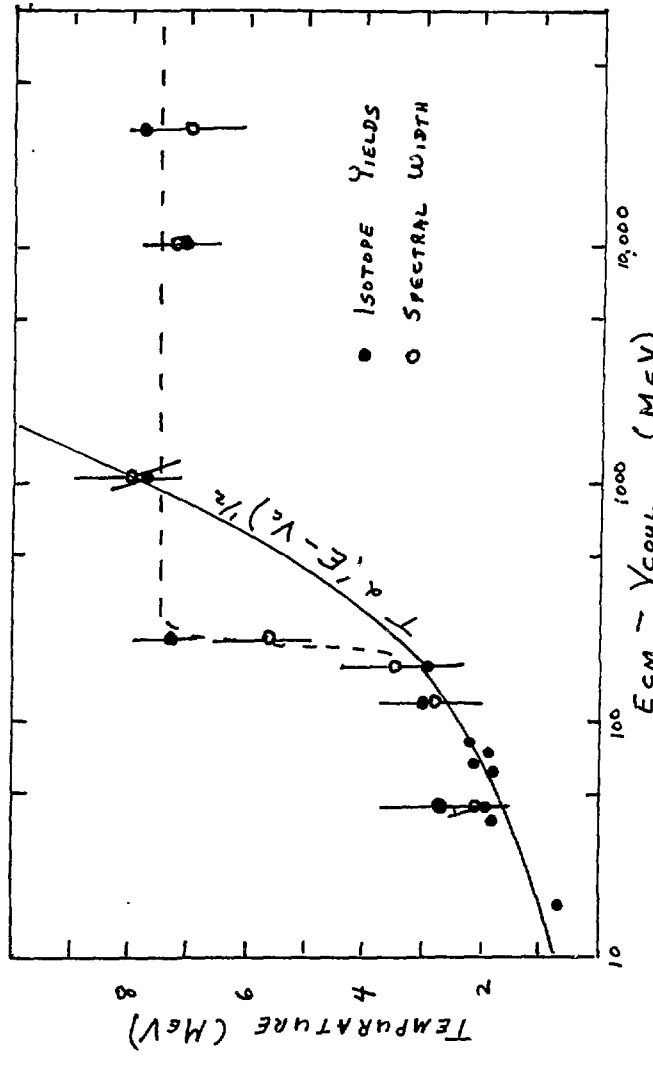

XBL 7711-10867

Fig. 15